CHEMISTRY OF MATERIALS
Article

Chem. Mater. **2010,** *22,* 4625–4631 4625
DOI:10.1021/cm100660v

Two-Dimensional $S = 1$ Quantum Antiferromagnet $(NiCl)Sr_2Ta_3O_{10}$

Yoshihiro Tsujimoto,[†,‡] Atsushi Kitada,[†,‡] Yasutomo J. Uemura,[§] Tatsuo Goko,[⊥] Adam A. Aczel,[#] Travis J. Williams,[#] Graeme M. Luke,[#] Yasuo Narumi,[||,▽] Koichi Kindo,[||] Masakazu Nishi,[||] Yoshitami Ajiro,[†] Kazuyoshi Yoshimura,[‡] and Hiroshi Kageyama*[,†,‡]

[†]*Department of Energy and Hydrogencarbon Chemistry, Graduate School of Engineering, Kyoto University, Kyoto, 615-8510, Japan,* [‡]*Department of Chemistry, Graduate School of Science, Kyoto University, Kyoto 606-8502, Japan,* [§]*Department of Physics, Columbia University, New York, New York 10027,* [⊥]*TRIUMF, Vancouver, British Columbia, Canada V6T 2A3,* [#]*Department of Physics and Astronomy, McMaster University, Hamilton, Ontario, Canada L8S 4M1,* [||]*Institute for Solid State Physics, The University of Tokyo, Kashiwa, Chiba 277-8581, Japan, and* [▽]*Institute for Materials Research, Tohoku University, Katahira 2-1-1, Sendai 980-8577, Japan*

Received March 4, 2010. Revised Manuscript Received July 10, 2010

A topotactic ion-exchange reaction of a layered perovskite $RbSr_2Ta_3O_{10}$ with $NiCl_2$ yielded a novel two-dimensional nickel-oxyhalide $(NiCl)Sr_2Ta_3O_{10}$, the first $S = 1$ compound among related series of metal-oxyhalides. The room temperature structure is isostructural with $(CuCl)Ca_2Nb_3O_{10}$ adopting the space group $P4/mmm$. We found a possible structural transition at 230 K that does not lead to drastic changes in magnetic character such as nickel clustering. Despite a large Weiss temperature of $\theta = -125$ K, magnetic long-range order is significantly suppressed down to $T_{N1} \approx 50$ K because of two-dimensionality and strong frustration. The magnetically ordered state below T_{N1} has a partial volume fraction coexisting with a paramagnetic component, followed by complete long-range ordering below $T_{N2} = 20$ K. The reaction process and requirement will also be discussed.

Introduction

Topotactic low-temperature reactions such as (de)intercalation and ion-exchange reactions provide a rational preparation of structures of nonmolecular solids that are not accessible by conventional high-temperature solid-state reactions.[1,2] Among candidate materials used as a precursor for such reactions, the most intensively studied system is the Dion-Jacobson (DJ) type layered perovskite expressed as $\acute{A}[A_{n-1}B_nO_{3n+1}]$, where $\acute{A}$ is an alkali metal (K, Rb, ...), A is an alkaline earth or rare earth metal (Sr, La, ...), B is a tetra- or penta-valent d^0 transition metal (Ti, Nb, Ta, ...), and n is the number of perovskite layers (2, 3, ...).[2] Here, highly reactive alkali metal ions at the $\acute{A}$ site afford versatile modification of the composition and stoichiometry, while retaining the structural feature of the chemically inert perovskite unit $[A_{n-1}B_nO_{3n+1}]$. By exploiting such a synthetic process, a wide variety of new or improved chemical and physical functionalities including (photo)catalysis,[3] ionic conductivity[4] and superconductivity[5] have been developed.

About a decade ago, J. B. Wiley and his collaborators demonstrated the ion-exchange reaction of the $n = 2$ and 3 DJ phases with CuX_2 (X = Cl, Br) to yield new metastable compounds $(CuX)^+[A_{n-1}B_nO_{3n+1}]^-$, where the Cu^{2+} ions are octahedrally coordinated, bridging between two apical oxygen ions from the perovskite blocks and surrounded by four halogen ions that share edges with neighboring CuO_2X_4 octahedra, forming a $S = 1/2$ square lattice.[6] These cupric halides can be regarded as good two-dimensional (2D) quantum spin magnets because the magnetic CuX layers are separated by the nonmagnetic perovskite blocks with a distance of 12 Å and 16 Å for $n = 2$ and 3, respectively. Indeed, intriguing quantum phenomena have been reported, for example, a spin-disordered ground state and field-induced magnetic order in $(CuCl)LaNb_2O_7$,[7] stripe

*To whom correspondence should be addressed. Tel.: +81-75-383-2506. Fax: +81-75-383-2510. E-mail: kage@scl.kyoto-u.ac.jp.

(1) Takada, K.; Sakurai, H.; Takayama-Muromachi, E.; Izumi, F.; Dilanian, R. A.; Sasaki, T. *Nature* **2003**, *422*, 53. Gopalakrishnan, J. *J. Chem. Mater.* **1995**, *7*, 1265. Hayward, M. A.; Cussen, E. J.; Claridge, J. B.; Bieringer, M.; Rosseinsky, M. J.; Kiely, C. J.; Blundell, S. J.; Marshall, I. M.; Pratt, F. L. *Science* **2002**, *295*, 1882. Tsujimoto, Y.; Tassel, C.; Hayashi, N.; Watanabe, T.; Kageyama, H.; Yoshimura, K.; Takano, M.; Ceretti, M.; Ritter, C.; Paulus, W. *Nature* **2007**, *450*, 1062. Colin, J. −F.; Pralong, V.; Caignaert, V.; Hervieu, M.; Raveau, B. *Inorg. Chem.* **2006**, *45*, 7217.
(2) Schaak, R. E.; Mallouk, T. E. *Chem. Mater.* **2002**, *14*, 1471.
(3) Yoshimura, J.; Ebina, Y.; Kondo, J.; Domen., K *J. Phys. Chem.* **1993**, *97*, 1970. Liou, Y.-W.; Wang, C. M. *J. Electrochem. Soc.* **1996**, *143*, 1492.
(4) Toda, K.; Watanabe, J.; Sato, M. *Solid State Ionics* **1996**, *90*, 15.
(5) Nagai, I.; Abe, Y.; Kato, M.; Koike, Y.; Kakihara, M. *Solid State Ionics* **2002**, *151*, 265.
(6) Kodenkandath, T. A.; Lalena, J. N.; Zhou, W. L.; Carpenter, E. E.; Sangregorio, C.; Falster, A. U.; Simmons, W. B.; O'connor, C. J.; Wiley, J. B. *J. Am. Chem. Soc.* **1999**, *121*, 10743. Kodenkandath, T. A.; Kumbhar, A. S.; Zhou, W. L.; Wiley, J. B. *Inorg. Chem.* **2001**, *40*, 710.
(7) Kageyama, H.; Kitano, T.; Oba, N.; Nishi, M.; Nagai, S.; Hirota, K.; Viciu, L.; Wiley, J. B.; Yasuda, J.; Baba, Y.; Ajiro, Y.; Yoshimura, K. *J. Phys. Soc. Jpn.* **2005**, *74*, 1702. Kageyama, H.; Yasuda, J.; Kitano, T.; Totsuka, K.; Narumi, Y.; Hagiwara, M.; Kindo, K.; Baba, Y.; Oba, N.; Ajiro, Y.; Yoshimura, K. *J. Phys. Soc. Jpn.* **2005**, *74*, 3155. Kitada, A; Hiroi, Z.; Tsujimoto, Y.; Kitano, T.; Kageyama, H; Ajiro, Y.; Yoshimura, K. *J. Phys. Soc. Jpn.* **2007**, *76*, 093706.

Published on Web 07/27/2010

magnetic order in $(CuBr)LaNb_2O_7$,[8] a 1/3 magnetization plateau in $(CuBr)Sr_2Nb_3O_{10}$,[9] and quantum phase separation in the solid solution $(CuCl)La(Nb, Ta)_2O_7$.[10] However, little is understood about the physics behind these observations.

This synthetic strategy was then extended to the other 3d transition metals, yielding a series of new materials $(MCl)LaNb_2O_7$ ($M = Mn^{2+}$, Fe^{2+}, etc.) and $(FeCl)Ca_2Ta_3O_{10}$,[11−14] which provides an opportunity for systematically tuning the magnetism as a function of spin quantum number ($S = 3/2$ for V^{2+} and Co^{2+}, $S = 2$ for Cr^{2+} and Fe^{2+}, $S = 5/2$ for Mn^{2+}). Because of the more classical nature of the spins, these compounds are known to undergo rather conventional antiferromagnetic order at relatively high ordering temperatures, for example, $T_N = 54$ K for $(MnCl)LaNb_2O_7$ and $T_N = 78$ K for $(FeCl)LaNb_2O_7$.[12,13] Thus it would be interesting to investigate the $S = 1$ system because a substantial quantum effect is expected and also because it may bridge the gap between well-understood classical spin systems and far-less understood $S = 1/2$ quantum spin systems. An attempt to prepare $(NiCl)LaNb_2O_7$ having $S = 1$ by the reaction of $RbLaNb_2O_7$ with $NiCl_2$ at 325 K resulted in $Ni_{0.5}LaNb_2O_7$.[15] It was discussed that the insertion of 0.5Ni(II) instead of Ni(II)Cl is due to a low vapor pressure of $NiCl_2$. In the course of study to search for new $n = 3$ materials, we succeeded in synthesizing $(NiCl)Sr_2Ta_3O_{10}$. In the paper, we report on the synthesis, structure, and magnetic properties of the new nickel oxychloride.

Experimental Section

Synthesis. The parent material $RbSr_2Ta_3O_{10}$ was synthesized by conventional high-temperature solid-state reaction as reported in the literature.[9] Starting reagents Rb_2CO_3 (>99.99%), $SrCO_3$ (>99.99%), and Ta_2O_5 (>99.99%) were weighed and ground together with an agate mortar in an argon-filled glovebox. Here, a 25% excess of Rb_2CO_3 was used to compensate the loss due to its volatilization. Then the mixture was placed in an alumina crucible and heated in air under ambient pressure at 850 °C for 12 h and at 1100 °C for 24 h with intermediate grinding. The product was washed thoroughly with distilled water to remove the excess alkaline carbonate and dried overnight at 120 °C. Subsequently, $RbSr_2Ta_3O_{10}$ was thoroughly ground with 2-fold molar excess of $NiCl_2$ (99.99%) in the argon-filled glovebox and was hand-pressed into a pellet. The pellet was transferred to a vacuum line without exposure to air, sealed in an evacuated Pyrex tube ($<1 \times 10^{-3}$ Torr), and then heated for 7 days at 340 °C. The obtained material, light green in color, was isolated by washing with distilled water to eliminate the byproduct RbCl and the unreacted $NiCl_2$, and dried overnight at 120 °C.

We also examined ion-exchange reactions with $NiCl_2$ using other precursors $RbCa_2B_3O_{10}$ (B = Nb and Ta), $RbSr_2Nb_3O_{10}$, and $CsPb_2Nb_3O_{10}$ and $CsBa_2B_3O_{10}$ (B = Nb and Ta) in a temperature range of 340−400 °C. However, no reactions occurred even after 14 days; the powder X-ray diffraction (XRD) patterns after the reactions showed no change in comparison with the corresponding parent compounds.

Characterization. Powder XRD data were collected on a M18XHF diffractometer (Mac Science) with a graphite monochromator using CuKα radiation. The final product was investigated also by powder synchrotron XRD using the large Debye−Scherrer camera installed on BL02B2 at SPring-8 with $\lambda = 0.42293$ Å, where the sample was sealed in a glass capillary with 0.2 mm diameter. The synchrotron XRD data were analyzed by the Rietveld technique, using the program RIETAN2000.[16] Profile refinements utilized the pseudo-Voigt function. The weighting R factor (R_{wp}) and the Bragg R factor (R_I) are defined as the following profile, $R_{wp} = [\Sigma_i w_i(y_{io}-y_{ic})^2/\Sigma_i w_i y_{io}^2]$; and $R_I = \Sigma_k |I_{ko}-I_{kc}|/\Sigma_k I_{ko}$, where y_{io} and y_{ic} are the observed and calculated intensities, w_i is the weighting factor, and I_{ko} and I_{kc} are the observed and calculated integrated intensities.

The magnetic susceptibility of the final product was measured in an applied magnetic field of $H = 1$ T over the temperature range of $T = 2-350$ K using a SQUID magnetometer (Quantum Design, MPMS). High-field magnetization measurements were conducted at 1.3 K up to 55 T using an induction method with a multilayer pulse magnet installed at Institute for Solid State Physics, The University of Tokyo. Specific heat measurements were performed using a relaxation technique with a physical property measurement system (Quantum Design, PPMS) from 1.8 to 280 K in zero field. A hand-pressed pellet was mounted on an alumina plate with grease for better thermal contact.

Muon spin relaxation (μSR) measurements were carried out on the M20 surface muon beamline at TRIUMF in Vancouver. Spin-polarized positive muons were implanted in the powder samples, and the time histograms of the forward−backward asymmetry of the decay positrons were recorded. Details of the μSR methods are described elsewhere in the literature.[17]

Results and Discussion

Synthesis and Structure. The laboratory XRD study confirmed the crystallization of $RbSr_2Ta_3O_{10}$ having tetragonal cell parameters of $a = 3.8926(7)$ Å and $c = 15.2531(2)$ Å; these are consistent with the results reported in ref 9. The laboratory XRD patterns of the final product were readily indexed on the tetragonal cell

(8) Oba, N.; Kageyama, H.; Kitano, T.; Yasuda, J.; Baba, Y.; Nishi, M.; Hirota, K.; Narumi, Y.; Hagiwara, M.; Kindo, K.; Saito, T.; Ajiro, Y.; Yoshimura, K. *J. Phys. Soc. Jpn.* **2006**, *75*, 113601.
(9) Tsujimoto, Y.; Baba, Y.; Oba, N.; Kageyama, H.; Fukui, T.; Narumi, Y.; Kindo, K.; Saito, Y.; Takano, M.; Ajiro, Y.; Yoshimura, K. *J. Phys. Soc. Jpn.* **2007**, *76*, 063711. Tsujimoto, Y.; Kageyama, H.; Baba, Y.; Kitada, A.; Yamamoto, T.; Narumi, Y.; Kindo, K.; Nishi, M.; Carlo, J. P.; Aczel, A. A.; Williams, T. J.; Goko, T.; Luke, G. M.; Uemura, Y. J.; Ueda, Y.; Ajiro, Y.; Yoshimura, K. *Phys. Rev B* **2008**, *78*, 214410.
(10) Uemura, Y. J.; Aczel, A. A.; Ajiro, Y.; Carlo, J. P.; Goko, T.; Goldfeld, D. A.; Kitada, A.; Luke, G. M.; MacDougall, G. J.; Mihailescu, I. G.; Rodriguez, J. A.; Russo, P. L.; Tsujimoto, Y.; Wiebe, C. R.; Williams, T. J.; Yamamoto, T.; Yoshimura, K.; Kageyama, H. *Phys. Rev. B* **2009**, *80*, 174408. Kitada, A.; Tsujimoto, Y.; Kageyama, H.; Ajiro, Y.; Nishi, M.; Narumi, Y.; Kindo, K.; Ichihara, M.; Ueda, Y.; Uemura, Y. J.; Yoshimura, K. *Phys. Rev. B* **2009**, *80*, 174409.
(11) Viciu, L.; Caruntu, G; Royant, N.; Koenig, J.; Zhou, W. L.; Kodenkandath, T. A.; Wiley, J. B. *Inorg. Chem.* **2002**, *41*, 3385.
(12) Viciu, L.; Koenig, J.; Spinu, L.; Zhou, W. L.; Wiley, J. B. *Chem. Mater.* **2003**, *15*, 1480.
(13) Viciu, L.; Golub, C. O.; Wiley, J. B. *J. Solid. State. Chem.* **2003**, *175*, 88.
(14) Kageyama, H.; Viciu, L.; Caruntu, G.; Ueda, Y.; Wiley, J. B. *J. Phys.: Condens. Matter* **2004**, *16*, S585.
(15) Viciu, L.; Liziard, N.; Golub, V.; Kodenkandath, T. A.; Wiley, J. B. *Mater. Res. Bull.* **2004**, *39*, 2147.
(16) Izumi, F.; Ikeda, T. *Mater. Sci. Forum* **2000**, *321*, 198.
(17) Hayano, R. S.; Uemura, Y. J.; Imazato, J.; Nishida, N.; Yamazaki, T.; Kubo, R. *Phys. Rev. B* **1979**, *20*, 850.

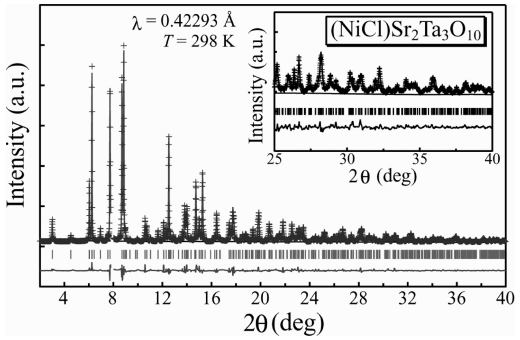

Figure 1. Rietveld refinement of the synchrotron XRD pattern for $(NiCl)Sr_2Ta_3O_{10}$ measured at room temperature: observed pattern (crosses), calculated pattern (solid line), difference curve (bottom solid line), and Bragg positions (tick marks).

Table 1. Crystallographic Data for $(NiCl)Sr_2Ta_3O_{10}$[a]

atom	site	x	y	z	sof[b]	U_{iso}(Å^2)
Ni	4*o*	0.096(3)	0	0.5	0.240(4)	0.027(5)
Cl	1*d*	0.5	0.5	0.5	1.00(2)	0.029(3)
Sr	2*h*	0.5	0.5	0.1401(2)	1	0.0069(4)
Tal	1*a*	0	0	0	1	0.0036(4)
Ta2	2*g*	0	0	0.2740(1)	1	0.0019(3)
O1	2*f*	0	0.5	0	1	0.07(1)
O2	2*g*	0	0	0.122(1)	1	0.008(4)
O3	4*i*	0	0.5	0.251(1)	1	0.003(2)
O4	2*g*	0	0	0.373(1)	1	0.004(4)

[a] Space group $P4/mmm$, a = 3.90185(4) Å, c = 16.1521(4) Å. R_{wp} = 6.38%, R_I = 1.42%. [b] sof = site occupancy factor.

Table 2. Selected Bond Lengths for $(NiCl)Sr_2Ta_3O_{10}$

bond	length (A)
Ni−Cl × 2	2.506(8)
× 2	3.037(1)
Ni−O4	2.08(2)
Tal−O1	1.9509(1)
Tal−O2	1.97(2)
Ta2−O2	2.42(2)
Ta2−O3	1.986(2)
Ta2−O4	1.59(2)

without any extinction conditions. The obtained lattice parameters, a = 3.895(2) Å and c = 16.100(3) Å are close to those for $(CuX)Sr_2Ta_3O_{10}$ (X = Cl and Br).[9,18] The nearly unchanged in-plane axes and the significantly elongated out-of-plane axis relative to the precursor are reminiscent of what have been found in related metal-halide compounds and are in sharp contrast to the case of $Ni_{0.5}LaNb_2O_7$, where the c axis contracts through the Rb^+-to-$Ni^{2+}{}_{0.5}$ exchange. These observations strongly suggest the ion-exchange between Rb^+ and $[Ni^{2+}-Cl^-]$, namely, the successful formation of $(NiCl)Sr_2Ta_3O_{10}$.

The synchrotron XRD data of the final product, performed at room temperature, confirmed the tetragonal structure without any additional reflections; this is consistent with the result of the laboratory XRD. The structural refinement assuming the structure of $(CuCl)Ca_2Nb_3O_{10}$ with the space group of $P4/mmm$[9] gave

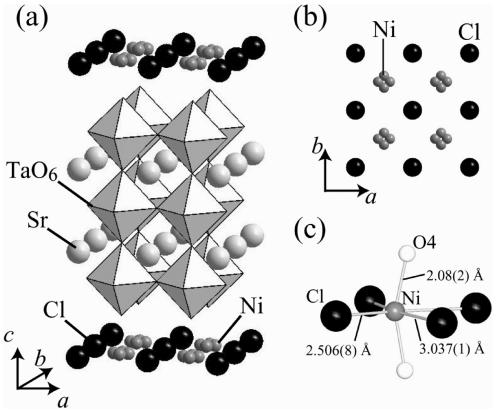

Figure 2. (a) Schematic crystal structure of $(NiCl)Sr_2Ta_3O_{10}$. Octahedron represents TaO_6. Black, small dark-gray, and large light-gray spheres represent chlorine, nickel, and strontium, respectively. The Ni ions are displaced to the 4*o* site. (b) The nickel-chlorine array viewed along [001]. (c) Local environment around the nickel ion that has two short and two long bonds with chlorines. The Ni is tetrahedrally coordinated with two oxygen atoms (white sphere) and two chlorine atoms.

reasonably small R factors of R_{wp} = 6.63% and R_I = 1.86%. However, the as-refined isotropic displacement parameter for the nickel site was extraordinary large (U_{iso} = 0.094(1) Å^2), implying that the nickel ions should move off the 1*b* site (0 0 1/2). Therefore, several models involving disorder of the nickel site were examined. Among them, the model in which the nickel ions occupy the 4*o* site (x, 0, 0.5) resulted in the best fit; the position of the Ni atom was slightly shifted to x = 0.096(3), the site occupancy factor (sof) for Ni was 0.240(4), being close to the full stoichiometry of 0.25, the U_{iso}(Ni) dropped to a reasonable value of 0.027(5) Å^2, and the reliability factors R_{wp} and R_I slightly decreased to 6.38% and 1.42%. We also examined several models where the chlorine site is disordered, but the chlorine atoms hardly moved off the original position 1*d* (0.5, 0.5, 0.5) indicating that no disorder occurs for the chlorine site. Observed, calculated, and difference plots are shown in Figure 1 and the structural parameters and selected bond lengths are listed in Tables 1 and 2. The crystal structure and the coordination environment around the nickel atom are illustrated in Figure 2.

We would like to note that, in common with quasi-isostructural ion-exchanged systems, a lattice mismatch between the host perovskite block and the inserted transition-metal halide array leads to the off-centering of either halide or transition-metal ions. The former occurs in M = Cu,[6,9] whereas the latter occurs in M = Fe[12] and the present-case Ni. For $(MnCl)LaNb_2O_7$, the disorder was suggested to occur for both Mn and Cl.[13] It is not clear at this stage why the metal-halide layer has so much variety in the site-occupations. Orbital states in the transition metal may be related to the modulating manner in the metal-halide layer. Also of interest is to check a superstructure formation, which was indeed found by the TEM (transmission electron microscopy) measurements for $(CuCl)LaNb_2O_7$.[19]

(18) Kageyama, H.; Kitano, T.; Nakanishi, R.; Yasuda, J.; Oba, N.; Baba, Y.; Nishi, M.; Ueda, Y.; Ajiro, Y.; Yoshimura, K. *Prog. Theor. Phys. Suppl.* **2005**, *159*, 39.

(19) Yoshida, M.; Ogata, N.; Takigawa, M.; Yamaura, J.; Ichihara, M.; Kitano, T.; Kageyama, H.; Ajiro, Y.; Yoshimura, K. *J. Phys. Soc. Jpn.* **2007**, *76*, 104703.

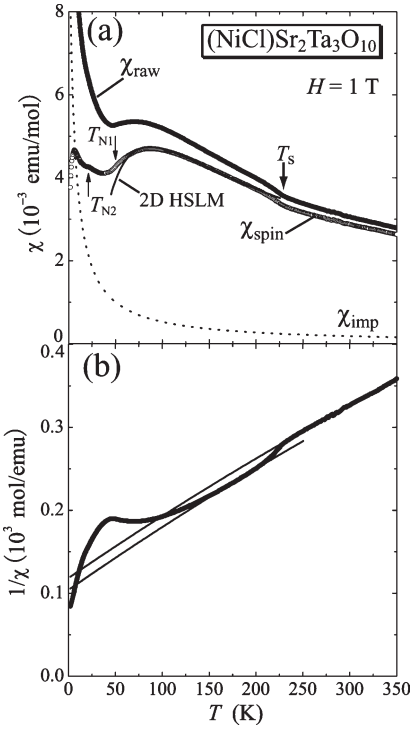

Figure 3. (a) The T dependence of the magnetic susceptibility at $H = 1$ T for (NiCl)$Sr_2Ta_3O_{10}$. The closed circles, open circles, and dotted line represent χ_{raw}, χ_{spin}, and χ_{imp}, respectively. The solid line on the data points between 50 and 200 K is a fit to an $S = 1$ Heisenberg square-lattice model (2D HSLM) obtained by high-temperature series expansion. (b) The inverse susceptibility vs T plot where the solid lines represent Curie−Weiss fits.

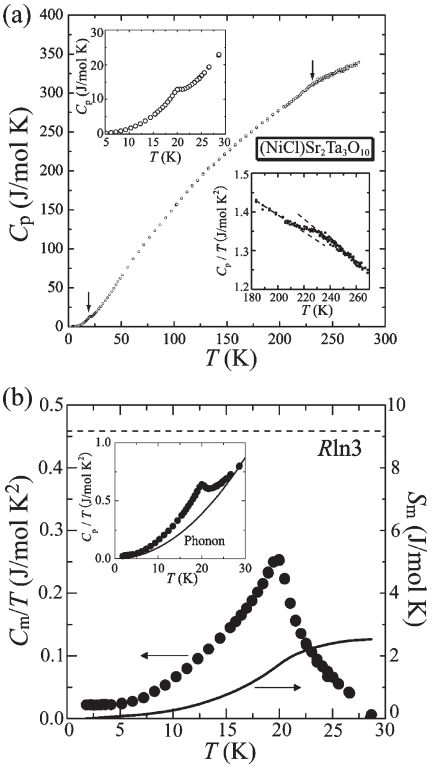

Figure 4. (a) The temperature dependence of the total heat capacity C_p at zero magnetic field. The bottom-right and top-left insets are C_p/T in $160 < T < 280$ K and C_p in $2 < T < 30$ K, respectively. (b) The magnetic heat capacity C_m/T and the magnetic entropy S_m. The inset shows the temperature dependences of C_p/T and the lattice contribution based on the Debye model with β (in βT^3) of 9.7×10^{-3} J/(K^4 mol).

Physical Properties. Let us hereafter assume the stoichiometric composition (NiCl)$Sr_2Ta_3O_{10}$ since the refined value of sof for Ni, 0.240(4), is nearly close to the ideal one. Figure 3 shows the temperature dependence of the molar magnetic susceptibility $\chi_{raw}(T)$ and its inverse $1/\chi_{raw}(T)$. There was no difference between zero-field cooling and field-cooling processes. A paramagnetic behavior observed above $T = 230$ K, was analyzed by the Curie−Weiss law including a T-independent term χ_0, which gave the Curie-constant $C = 1.14(5)$ emu K/mol, Weiss temperature $\theta = -144.0(1)$ K and $\chi_0 = 4.6(5) \times 10^{-4}$ emu K/mol. The value of C corresponds to that expected from 1 mol of Ni^{2+} ions with $g = 2.14$, supporting once again completion of the ion-exchange reaction. The large negative θ suggests strong antiferromagnetic interactions in the NiCl layer, a distinct feature different from $Ni_{0.5}LaNb_2O_7$ which exhibits a paramagnetic behavior down to 3 K with a small Weiss temperature of $\theta = -3.5$ K.[15] This means that the Cl ions in (NiCl)$Sr_2Ta_3O_{10}$ provide significant Ni−Cl−Ni superexchange pathways.

Interestingly, when temperature was further decreased, an anomaly appeared at around 230 K, which is likely to be a structural phase transition. As shown in Figure 4, the specific heat exhibited a hump at around $T_s = 230$ K, and this anomaly is more clearly seen when one plots C_p/T against T. This structural transition may be accounted for by octahedral rotation of the $Sr_2Ta_3O_{10}$ blocks, leading to a superstructure, as typically seen in perovskite related materials. Thus, we performed powder synchrotron XRD measurements at 100 K ($< T_s$), using the BL02B2 beam port in SPring-8. However, we could not observe any additional peaks associated with a superstructure formation and the Rietveld refinement provided essentially the same structure as that at room temperature. This experimental result is possibly due to the use of polycrystalline sample. In addition, because octahedral rotation in the perovskite blocks, if it happens at T_s, is related to displacement of oxygen sites, high-resolution neutron diffraction measurements should be more suitable, which will be performed in the near future. Ordering of nickel atoms in the NiCl layer may be an alternative origin of the structural transition. In this case, however, we see that the slope of $1/\chi_{raw}$ does not essentially change upon this transition: the curve with $C = 1.14$ emu K/mol and $\theta = -125(5)$ K, $\chi_0 = 4.6 \times 10^{-4}$ emu K/mol well-reproduces the experimental curve, although it is difficult to perform the Curie−Weiss fitting given a short range of temperature having a straight slope. It follows that the compound stays in a paramagnetic state below T_s and that even if nickel atoms become ordered, it does not lead to any clustering of magnetic atoms such as tetramering and trimering as found in $La_4Cu_3MoO_{12}$ does not occur because otherwise the slope in $1/\chi$ would become steeper.[20]

(20) Azuma, M.; Odaka, T.; Takano, M.; Vander Griend, D. A.; Poeppelmeier, K. R.; Narumi, Y.; Kindo, K.; Mizuno, Y.; Maekawa, S. *Phys. Rev. B* **2000**, *62*, R3588.

On further cooling, a deviation from the Curie−Weiss behavior becomes appreciable, indicative of development of short-range spin correlations in the NiCl layer. A broad maximum in χ_{raw} at $T_\chi^{max} = 70$ K is characteristic of low-dimensional antiferromagnets. The Curie tail below 50 K should be due to paramagnetic spins associated with small amount of defects or impurities. However, this component could not be satisfactorily subtracted using a simple Curie equation. We therefore estimated this extrinsic term by the Curie−Weiss equation $\chi_{imp} = C_{imp}/(T - \theta_{imp})$ as sometimes used in low-dimensional spin systems such as LiV_2O_5 (−5.1 K),[21] $SrCu_2(BO_3)_2$ (− 2.5 K)[22] and $InCu_{2/3}V_{1/3}O_3$ (−10 K).[23] A better agreement was obtained for $\theta_{imp} = -4.8$ K and $C_{imp} = 0.055$ emu K/mol. The obtained value of C_{imp} corresponds to 5.5% of $S = 1$ spins. Interestingly, the corrected susceptibility $\chi_{spin}(T)$, $\chi_{raw}(T) - \chi_{imp}(T)$, showed a tiny kink at 20 K. This temperature coincides with the temperature, at which a λ-type anomaly in the specific heat C_p was seen (Figure 4a). As will be confirmed later, this anomaly can be attributed to magnetic order. A magnetic heat capacity C_m was estimated by subtracting a lattice contribution using the Debye model with βT^3. Because there is no isostructural nonmagnetic material currently available, $\beta = 9.7 \times 10^{-3}$ J/(K^4 mol) obtained for the triple-layered $(CuBr)Sr_2Nb_3O_{10}$ was employed here.[9] The magnetic entropy S_m at 30 K, obtained by T-integrating C_m/T, is only 30% of the total magnetic entropy Rln 3, presumably reflecting two-dimensionality and competing magnetic interactions.

To further characterize the phase transition at 20 K, we conducted μSR measurements, a useful technique to detect magnetic order with high sensitivity.[24] Figure 5 shows the time spectra of zero-field μSR(ZF-μSR) in $(NiCl)Sr_2Ta_3O_{10}$ at low temperatures. The corrected asymmetry at 1.4 K showed an oscillating behavior, providing firm evidence for long-range magnetic order. What is remarkable is that this oscillation retained even above 20 K ($= T_{N2}$) (see the 25 and 45 K spectra), the temperature at which the λ-type anomaly in $C_p - T$ was detected, indicating persistence of the magnetic order at temperatures above 20 K. The spectra above 50 K showed no oscillation, but the fast decay was still present at 50 K (Figure 5b). No fast decay is seen for the spectra for $T \geq 60$ K. The accurate value of the transition temperature into a paramagnetic state ($= T_{N1}$) is difficult to define: 50 K is the safe lower limit and 60 K is the upper limit.

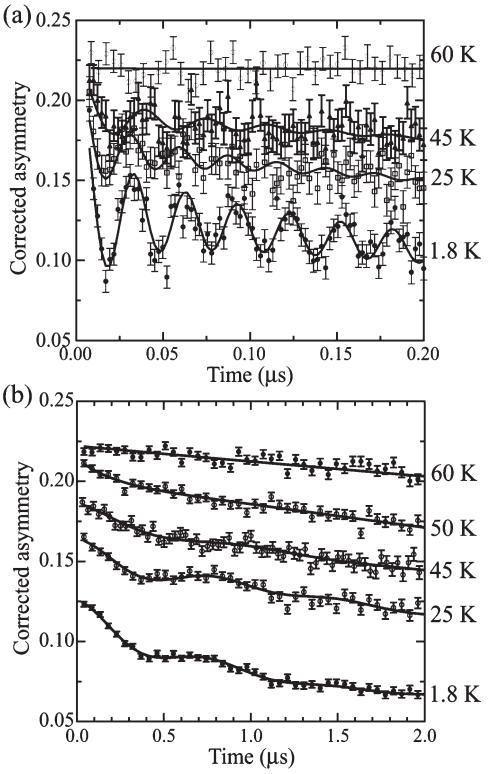

Figure 5. Time evolution of zero-field μSR asymmetry measured at each temperature. Note that the time scales in two plots are different between (a) and (b). Solid curves are the fit to eq 1.

The time spectra were analyzed by fitting to a combination of four signals (Figure 5);

$$G_z(t) = A_1\exp(-\lambda_1 t)J_0(2\pi\nu_1 t + \varphi_i) + A_2\exp(-\lambda_2 t)J_0(2\pi\nu_2 t + \varphi_2) + A_3\exp(-1/2\sigma_3{}^2 t^2) + A_4\exp(-\lambda_4 t) \quad (1)$$

where $A_i (i = 1, 2, 3, 4)$ is the asymmetry, $\nu_i (\nu_1 > \nu_2)$ is the muon spin precession frequency, λ_i and σ_3 are the relaxation rates, and $J_0(2\pi\nu_i t + \varphi_i)$ is a zeroth-order Bessel function with an initial phase φ_i which is widely used to describe an incommensurate spin density wave state.[25] The first two terms represent the oscillating components from muons experiencing static internal fields, the third term represents a Gaussian relaxing signal from a random static field, and the last term represents signals uninvolved in the ordered volume fraction, namely, contributions from both a paramagnetic volume fraction and the muons stopping at a site where the local static field is parallel to the initial spin polarization. Figure 6a shows the presence of two frequencies, ν_1 and ν_2, likely ascribed to inequivalent magnetic muon sites. A_i's are plotted as a function of temperature in Figure S1 in the Supporting Information. A_1, A_2, and A_3 associated with magnetic

(21) Isobe, M.; Ueda, Y. *J. Phys. Soc. Jpn.* **1996**, *65*, 3142.
(22) Kageyama, H.; Yoshimura, K.; Stern, R.; Mushnikov, N. V.; Onizuka, K.; Kato, M.; Kosuge, K.; Slichter, C. P.; Goto, T.; Ueda, Y. *Phys. Rev. Lett.* **1999**, *82*, 3168.
(23) Kataev, V.; Möller, A.; Löw, U.; Jung, W.; Schittner, N.; Kriener, M.; Freimuth, A. *J. Magn. Magn. Mater.* **2005**, *290−291*, 310.
(24) Kojima, K.; Keren, A.; Luke, G. M.; Nachumi, B.; Wu, W. D.; Uemura, Y. J.; Azuma, M.; Takano, M. *Phys. Rev. Lett.* **1995**, *74*, 2812. Kojima, K. M.; Fudamaoto, Y.; Larkin, M.; Luke, G. M.; Merrin, J.; Nachumi, B.; Uemura, Y. J.; Motoyama, N.; Eisaki, H.; Uchida, S.; Yamada, K.; Endoh, Y.; Hosoya, S.; Sternlieb, B. J.; Shirane, G. *Phys. Rev. Lett.* **1997**, *78*, 1787. Ohishi, K.; Yamada, I.; Koda, A.; Higemoto, W.; Saha, S.; Kadono, R.; Kojima, K. M.; Azuma, M.; Takano, M. *J. Phys. Soc. Jpn.* **2005**, *74*, 2408.
(25) Le, L. P.; Keren, A.; Luke, G. M.; Sternlieb, B. J.; Wu, W. D.; Uemura, Y. J.; Brewer, J. H.; Riseman, T. M.; Upasani, R. V.; Chiang, L. Y.; Kang, W.; Chaikin, P. M.; Csiba, T.; Günter, G. *Phys. Rev. B* **1993**, *48*, 7284. Sugiyama, J.; Ikedo, Y.; Mukai, K.; Brewer, J. H.; Ansaldo, E. J.; Morris, G. D.; Chow, K. H.; Yoshida, H.; Hiroi, Z. *Phys. Rev. B* **2006**, *73*, 224437.

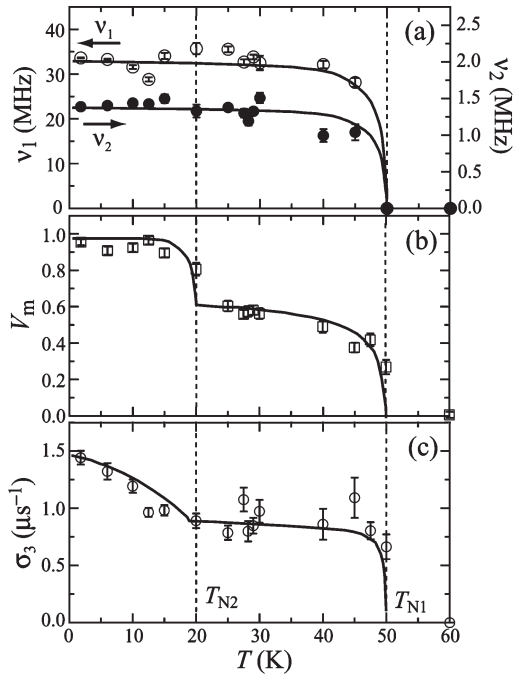

Figure 6. The temperature dependence of (a) the ordered volume fraction V_m obtained from eq 1. See the Supporting Information for detail. (b) Temperature dependences of the muon precession frequencies ν_1 and ν_2 in the first and second terms, (c) the relaxation rate σ_3 in the third term of eq 1. Solid curves are guides to the eye.

order grew with decreasing temperature below 50 K. Shown in Figure 6b is the ordered volume fraction $V_m = (A_1 + A_2 + A_3) \times (3/2)/(A_1 + A_2 + A_3 + A_4)$ (see the Supporting Information for detail), which exhibited a characteristic stepwise temperature dependence; with decreasing temperature, V_m showed a plateau with 60% of the full volume fraction, jumps at around T_{N2}, and saturated to the full volume fraction. The temperature dependence of σ_3 shown in Figure 6c also exhibited a stepwise increment.

What the intermediate magnetic state looks like? We consider that some spins in this state can fluctuate presumably because of spin frustration, as observed in triangular antiferromagnets $CsCoX_3$ (X = Cl, Br).[26] Further experiments using nuclear resonance or neutron scattering are necessary to clarify the nature of the intermediate as well as the ground state of (NiCl)$Sr_2Ta_3O_{10}$.

In the case of related cupric chloride materials, the existence of competing interactions has been proposed.[7−10] The competing magnetic interactions may be also present in (NiCl)$Sr_2Ta_3O_{10}$ as seen from the unusual temperature dependence of V_m in the μSR study. It would be nevertheless helpful to roughly estimate the magnitude of magnetic interactions using a simple, noncompeting 2D Heisenberg square-lattice model taking only the nearest neighbor interaction into account. We

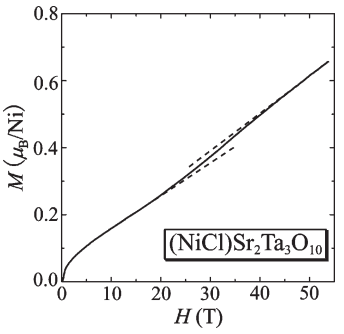

Figure 7. High-field magnetization of (NiCl)$Sr_2Ta_3O_{10}$ measured up to 55 T at 1.3 K.

employed a high-temperature series expansion to our susceptibility data,[27]

$$\frac{Ng^2\mu_B{}^2}{\chi J} = 3\xi + \sum_{n=1}^{6} \frac{C_n}{\xi^{n-1}} \qquad (2)$$

where N is the Avogadro constant, J is the nearest-neighbor exchange constant, k_B is the Boltzmann constant, $\xi = k_BT/JS(S+1)$, the C_n coefficients are $C_1 = 4$, $C_2 = 1.834$, $C_3 = 0.445$, $C_4 = 0.224$, $C_5 = 0.132$, $C_6 = 0.019$.[27] In fitting, a T-independent term, χ_0, was included as diamagnetic and Van Vleck contributions to χ and the value of g estimated from the Curie−Weiss fit was used. As shown in Figure 3a, the fitting above 60 K resulted in $J/k_B = 39.32(7)$ K and $\chi_0 = 3.0(1) \times 10^{-4}$ emu/mol. The exchange constant can be also estimated using the equation $k_BT_\chi{}^{max}/J = 1.12S(S + 1)$ in the 2D Heisenberg square-lattice model,[27] which resulted in $J/k_B = 38$ K, being close to the exchange constant estimated above. The obtained exchange constant is much stronger than those in (MCl)$LaNb_2O_7$ ($J/k_B = 3.77$ K for M = Mn and 7.78 K for M = Fe).[12,13]

Reflecting the substantial antiferromagnetic interactions derived from the Weiss temperature, the magnetization $M(H)$ at 1.3 K (Figure 7) grew gradually, reaching 0.6 μ_B at 55 T, only 30% of the saturation magnetization of Ni^{2+} (2 μ_B). A convex curvature as seen below 3 T should originate from the paramagnetic impurities. The linear evolution of the magnetization in the low field range was followed by the spin-flop transition at $H_c = 20$ T. This phenomenon is observed for geometrically frustrated antiferromagnets such as $CsNiCl_3$ and K_2NiF_4 with easy-axis anisotropy coming from single-ion anisotropy that is allowed to be nonzero for $S > 1/2$.[28−30] Thus, our compound might experience competing or frustrated interaction as already pointed out in related oxyhalides.[7−10]

On the Reaction Mechanism. Some conditions and mechanisms that allow insertion of metal-halide arrays in between perovskite layers have been discussed so far. For example, a faster reaction rate of (CuCl)LaB_2O_7 with

(26) Yelon, W. B.; Cox, D. E.; Eibschütz, M. *Phys. Rev. B* **1975**, *12*, 5007. Mekata, M.; Adachi, K. *J. Phys. Soc. Jpn.* **1978**, *44*, 806. Mekata, M.; Okamoto, S.; Onoe, S.; Ajiro, Y.; Kikuchi, H.; Inami, T.; Torikai, E.; Nagamine, K. *Hyperfine Interact.* **1990**, *59*, 415.
(27) Lines, M. E. *J. Phys. Chem. Solids.* **1970**, *31*, 101.
(28) Johnson, P. B.; Rayne, J. A.; Friedberg, S. A. *J. Appl. Phys.* **1979**, *50*, 1853.
(29) Matsuura, M.; Gilijamse, K.; Sterkenburg, J. E. W.; Breed, D. J. *Phys. Lett.* **1970**, *33A*, 363.
(30) Collins, M. F.; Petrenko, O. A. *Can. J. Phys.* **1997**, *75*, 605.

$LiLaB_2O_7$ than with $RbLaB_2O_7$ was attributed to the mobility of alkali-metal cation (Li > Rb), while the importance of the interlayer space of the precursor was inferred from the capability/incapability to prepare $(CuBr)LaB_2O_7$ from the $RbLaNb_2O_7/LiLaNb_2O_7$ precursor. In addition, ion-exchangeability may be influenced by pliability of each perovskite slab $[A_{n-1}B_nO_{3n+1}]^-$ because the ion-exchange reaction proceeds from the side edge of the particle of the precursor toward its central part and the reaction involves a significant increase in the out-of-plane lattice of the order of 1 Å. It is intuitively expected that the $[A_{n-1}B_nO_{3n+1}]^-$ blocks become harder with increasing n, and this feature might provide apparent explanation of why the triple layer analogues of $(M\text{Cl})LaNb_2O_7$ (M = V, Cr, Mn, and Co)[11] could not be obtained (not shown). However, it is demonstrated in the present study that the insertion of NiCl layer does not occur in double layered system but triple-layered one with the particular set of A = Sr and B = Ta. This inconsistent result with the above hypothesis will call for further inspections of the mechanism of related ion-exchange reaction.

Here we would like to address several points. First, the low vapor pressure of $NiCl_2$ does not necessarily become the factor to block the insertion of the "Ni−Cl" layer instead of the "$Ni_{0.5}$" layer because the $Ni_{0.5}A_2B_3O_{10}$ phase is not formed. Second, the failed insertion of the NiCl layer for other triple-layered compounds with different sets of A and B indicates the necessity to look at the structure in an atomic scale. For example, octahedral distortions and rotations, generally observed in perovskite and its related oxides depending on the size of the A site, may influence the ability of the perovskite block to bend, and the difference in the electronegativity between Nb and Ta might also affect the reactivity with $NiCl_2$. It is also considered that transient coordination number and geometry around a Ni atom at the interface between $RbSr_2Ta_3O_{10}$ and $(NiCl)Sr_2Ta_3O_{10}$ are likely to be stable, hence pushing the reaction forward. Investigations of the precise structure by using (in situ) TEM and single crystalline XRD and the local coordination during the reaction are beyond the scope of this study, but such studies should be important issues for the future.

Conclusion

Using the ion-exchange reaction, we obtained a two-dimensional S = 1 square-lattice system $(NiCl)Sr_2Ta_3O_{10}$, which is the first example of S = 1 among related layered systems. The disorder of the Ni atoms from the ideal position to (x 0 1/2) was inferred from the structural analysis at room temperature. A structural transition at 230 K might involve octahedral tilting of perovskite blocks and/or a certain rearrangement of the NiCl layers. As a characteristic feature of the two-dimensional quantum antiferromagnet, the magnetic susceptibility shows a broad maximum at 70 K. The μSR measurements evidenced the successive magnetic phase transitions at T_{N1} = 50 K and T_{N2} = 20 K. However, a partial paramagnetic volume fraction remains in the intermediate phase. In addition, a spin flop transition at H_c = 20 T was observed in the high-field magnetization measurements. It is therefore of particular interest to investigate and compare the magnetic properties of the whole family $(MX)A_{n-1}B_nO_{3n+1}$ from both experimental and theoretical points of view.

The previous and present results on the preparation of layered metal-oxyhalides shed light on the importance of viewing the reaction process in detail, especially because those reactions occur at relatively low-temperatures. We believe that knowledge obtained from such studies is useful to understand the diffusion process in ion-conductors and to design other inorganic materials by low-temperature reactions.

Acknowledgment. This work was supported by Grants-in-Aid for Science Research on Priority Areas "Novel States of Matter Induced by Frustration" (19052004) from the Ministry of Education, Culture, Sports, Science and Technology of Japan, the Japan−U.S. Cooperative Science Program from JSPS of Japan and NSF (14508500001), and by the Global COE program International Center for Integrated Research and Advanced Education in Material Science, Kyoto University, Japan. The work at Columbia University was supported by U.S. NSF Grants DMR-05-02706 and DMR-08-06846. The work at McMaster University was supported by NSERC and CIFAR. This work is also partly supported by the Japan Society for the Promotion of Science (JSPS) through its "Funding Program for World-Leading Innovative R&D on Science and Technology (FIRST) Program". One of the authors (Y.T.) was supported by the Japan Society for the Promotion of Science for Young Scientists.

Supporting Information Available: Temperature dependence of each asymmetry A_i (i = 1, 2, 3, and 4) and definition of the magnetic volume fraction V_m (PDF). This material is available free of charge via the Internet at http://pubs.acs.org."